Fluctuation mediated phase separation in polymer blends near the limit of metastability

A. A. Lefebvre and J. H. Lee
Department of Chemical Engineering, University of California, Berkeley, California 94720

N. P. Balsara
Department of Chemical Engineering, University of California, Berkeley, California 94720 and Materials Sciences Division, Lawrence Berkeley National Laboratory, University of California, Berkeley, California 94720

C. Vaidyanathan
Department of Chemical Engineering, Chemistry and Materials Science, Polytechnic University, Brooklyn, New York 11201

(Received 20 June 2002; accepted 9 August 2002)

The evolution of the structure factor of off-critical polyolefin (polymethylbutylene/polyethylbutylene) blends quenched from the homogeneous state to states near the limit of metastability was studied by small angle neutron scattering. The Cahn–Hilliard–Cook theory was used to organize the data in terms of three time-independent parameters that depend on the scattering vector, q: $S_0(q)$, the initial structure factor, $S_t(q)$, the terminal structure factor, and $R(q)$, a kinetic parameter that indicates the time scale for the transformation from $S_0(q)$ to $S_t(q)$. These three parameters change systematically with quench depth. Changes in the structure factor $S(q,t)$ are only observed in the q values smaller than a critical scattering vector, q_c. At small quench depths, q_c is obtained because $R(q)\rightarrow 0$ as $q\rightarrow q_c$. At deeper quenches, q_c is obtained because $S_t(q)\rightarrow S_0(q)$ as $q\rightarrow q_c$. Scattering characteristics at $q<q_c$ such as scattering peaks or the lack thereof arise due to the interplay between $R(q)$ and $S_t(q)$. © *2002 American Institute of Physics.* [DOI: 10.1063/1.1511513]

I. INTRODUCTION

This paper builds on the preceding paper,[1] where the early stages of phase separation in high molecular weight polymer blends were studied by time-resolved small angle neutron scattering (SANS). Our objective was to study the formation of critical nuclei during the transformation of a metastable homogeneous mixture to a stable two-phase mixture. We thus studied blends that were located between the binodal and spinodal curves calculated on the basis of the Flory–Huggins theory. We found that scattering profiles obtained during the early stages of phase separation merged at a critical scattering vector, q_c. We argued that the critical (smallest) length scale of the growing structures was $R_c \sim 1/q_c$. The purpose of this paper is to focus on changes in the scattering profiles at $q<q_c$ and thereby study the characteristics of structures larger than R_c. The experimentally determined dependence of R_c on quench depth differed substantially from predictions based on classical theories.[2] An explanation of these differences was recently offered by the theoretical work of Wang and Wood[3,4] who predict that the regime over which thermodynamics is affected by concentration fluctuations (also known as the Ginzburg regime) is much wider than previously envisaged. They concluded that the data obtained in Ref. 1 was located within the Ginzburg regime. Phase separation in systems near the critical point, where fluctuations play a dominant role, is often described by the Cahn–Hilliard–Cook (CHC) theory.[5–7] Since it has been established by both experiments[1,8–10] and theory[3,4] that fluctuations play a dominant role in the series of blends that we have studied, we decided to use the CHC theory to fit the time dependence of the scattering profiles observed at $q<q_c$. We find that the CHC theory provides an excellent starting point for organizing the data. It also provides insight into the origin of the critical scattering vector, q_c.

II. EXPERIMENT

We discuss experiments conducted on a binary polymethylbutylene/polyethylbutylene (PMB/PEB) blend, designated B3. All of the experimental details are given in Ref. 1. The data from B1 and B2 (the other blends studied in Ref. 1) were also analyzed using methods described here, and these results agree with our conclusions. For brevity, we only discuss data obtained from B3.

III. THEORETICAL FRAMEWORK FOR DATA ANALYSIS

The SANS intensity from a polymer blend at a given T and P is[11]

$$I(q,t)=\left(\frac{b_1}{v_1}-\frac{b_2}{v_2}\right)^2\times S(q,t), \tag{1}$$

where b_i is the neutron scattering length of the monomer in polymer chain i with a monomer volume v_i, and $S(q,t)$ is the structure factor of the blend.

If the blend is at equilibrium, the structure factor, $S_{\mathrm{RPA}}(q)$, in the mean field limit is time-independent, and given by the random phase approximation (RPA),[12–14]

$$S_{\mathrm{RPA}}(q)=\left(\frac{1}{N_1 v_1 \phi_1 P_1(q)}+\frac{1}{N_2 v_2 \phi_2 P_2(q)}-\frac{2\chi}{v_0}\right)^{-1}, \tag{2}$$

where N_i is the number of monomer units with a volume v_i in polymer chain i, ϕ_i is the volume fraction of polymer i, P_i is the Debye function of polymer chain i, χ is the Flory–Huggins interaction parameter, and v_0 is a reference volume, which for this work is equal to 100 Å^3. The Debye function is given by

$$P_i(q)=\frac{2}{x^2}(e^{-x}+x-1), \tag{3}$$

where $x=q^2 Rg_i^2$, $Rg_i^2=N_i l_{i,\mathrm{ref}}^2/6$, and $l_{i,\mathrm{ref}}$ is the statistical segment length of polymer i (see Ref. 1 for values of the parameters).

In the Cahn–Hilliard–Cook (CHC) theory,[5–7] the evolution of the structure factor, $S(q,t)$, after the sample is quenched from an initial equilibrium state at $t=0$ with a structure factor $S_0(q)$, is given by

$$S(q,t)=S_t(q)+[S_0(q)-S_t(q)]\exp[2R(q)t], \tag{4}$$

where $S_t(q)$ is the terminal structure factor obtained in the $t\to\infty$ limit, and $R(q)$ is a kinetic parameter that is related to the growth [if $R(q)$ is positive] or decay [if $R(q)$ is negative] of $S_0(q)$. For convenience, we define

$$\Delta S(q)=S_0(q)-S_t(q). \tag{5}$$

The time-dependence of $S(q,t)$ in Eq. (4) is thus governed by three q-dependent parameters, $R(q)$.

It has been shown that the CHC theory [Eq. (4)] is applicable to quenches from one single-phase equilibrium state to another.[15,16] In this case, $S_t(q)$ is positive at all values of q because the terminal state is at equilibrium, and $R(q)$ is negative at all q. Equation (4) thus describes a smooth transition from $S_0(q)=S_{\mathrm{RPA}}(q)$ of the initial state to $S_t(q)=S_{\mathrm{RPA}}(q)$ of the quenched state. When blends are quenched from the single-phase state into the unstable region,[17–24] Eq. (4) applies to the early stages of spinodal decomposition. In this regime, $R(q)$ is positive over a range of q values indicating exponential growth of concentration fluctuations with certain characteristic lengths. The growth rate is maximum at a finite scattering vector, q_p, giving rise to the familiar peak in the scattering intensity profile during spinodal decomposition. $S_t(q)$ for unstable blends is negative in the range $q<q_c$, positive at $q>q_c$, and contains a pole at $q=q_c$. $S_t(q)$ is often called the virtual structure factor due to the presence of negative values and a singularity.[17] For sufficiently deep quenches, $S_0(q)\gg S_t(q)$ in the vicinity of q_p and Eq. (4) reduces to the well-known Cahn–Hilliard equation,[8,12,17,25–28]

$$S(q,t)=S_0(q)\exp[2R_{\mathrm{CH}}(q)t]. \tag{6}$$

IV. RESULTS AND DISCUSSION

A series of phase separation experiments were performed using the blend, B3, at 58 °C and various pressures between 0.86 and 3.10 kbar, within the metastable region of the mean-field phase diagram. For simplicity we will refer to each quench by the quench pressure only, since the quench temperature was always 58 °C. The time evolution of the SANS intensity profiles for the different quenches is shown in Figs. 1(a)–1(d). A variety of behaviors are seen as a function of quench depth. A deep quench [Fig. 1(a)] to 3.10 kbar leads to a well-defined scattering peak. The location of the peak in q-space is independent of time for the duration of the experiment (294 min). Shallower quenches to 2.00 kbar [Fig. 1(b)] lead to the development of scattering peaks that move to lower q values with increasing time. The quench to 1.24 kbar [Fig. 1(c)] leads to scattering profiles without peaks. The shallowest quench to 0.86 kbar [Fig. 1(d)] results in no change in the scattering intensity for the duration of the experiment (911 min). In the remainder of the paper we focus on the data obtained at larger quench depths [Figs. 1(a)–1(c)].

For all of the data, the structure factor $S(q,t)$ is calculated from $I(q,t)$ using Eq. (1) and b_i and v_i values given in Ref. 1. In Fig. 2 we show the time dependence of $S(q,t)$ at $q=0.021$ nm^{-1} for the shallow quench to 1.24 kbar. In this experiment, we see the three stages of phase separation described in Ref. 1: a fluctuation relaxation stage where $S(q,t)$ increases rapidly with time at $t<\tau_F$, an early stage where $S(q,t)$ increases slowly with time for $\tau_F\leqslant t\leqslant\tau_E$, and a late stage where $S(q,t)$ increases rapidly again at $t>\tau_E$. Identification of the end of both the fluctuation relaxation (τ_F) and early (τ_E) stages was discussed in detail in Ref. 1, and are shown by the arrows in Fig. 2. For the deeper quenches ($P>1.24$ kbar) we observed only the early and late stages.

For the 1.24 kbar quench, we define τ_F as the beginning of the early stage. It is evident from Fig. 2 that the crossover between the early and late stage is gradual. Thus, it is difficult to determine the exact end of the early stage of phase separation. For this work, we define the end of the early stage, τ_E', as the last time at which the CHC theory can be applied to the data. In Fig. 2 we show the result of the fit of the CHC theory [Eq. (4)] to $S(q,t)$ between τ_F (47 min) $\leqslant t\leqslant$664 min for the 1.24 kbar quench. In this time period the CHC theory describes the change in $S(q,t)$ well. At later times, however, we find significant deviations between the measured $S(q,t)$ and the CHC theory. Thus, for this quench $\tau_E'=664$ min.

For the deeper quenches ($P>1.24$ kbar), we see the development of a scattering peak at q_p, indicating the formation of a periodic structure with a characteristic length scale of $1/q_p$ [Figs. 1(a) and 1(b)]. The location of the scattering peak is determined by fitting a Gaussian curve to the ten points closest to the estimated scattering peak,

$$I=I_p\exp\left(\frac{-2(q-q_p)^2}{\sigma^2}\right), \tag{7}$$

where I_p and σ are measures of peak intensity and width, respectively. The time dependence of the peak position q_p

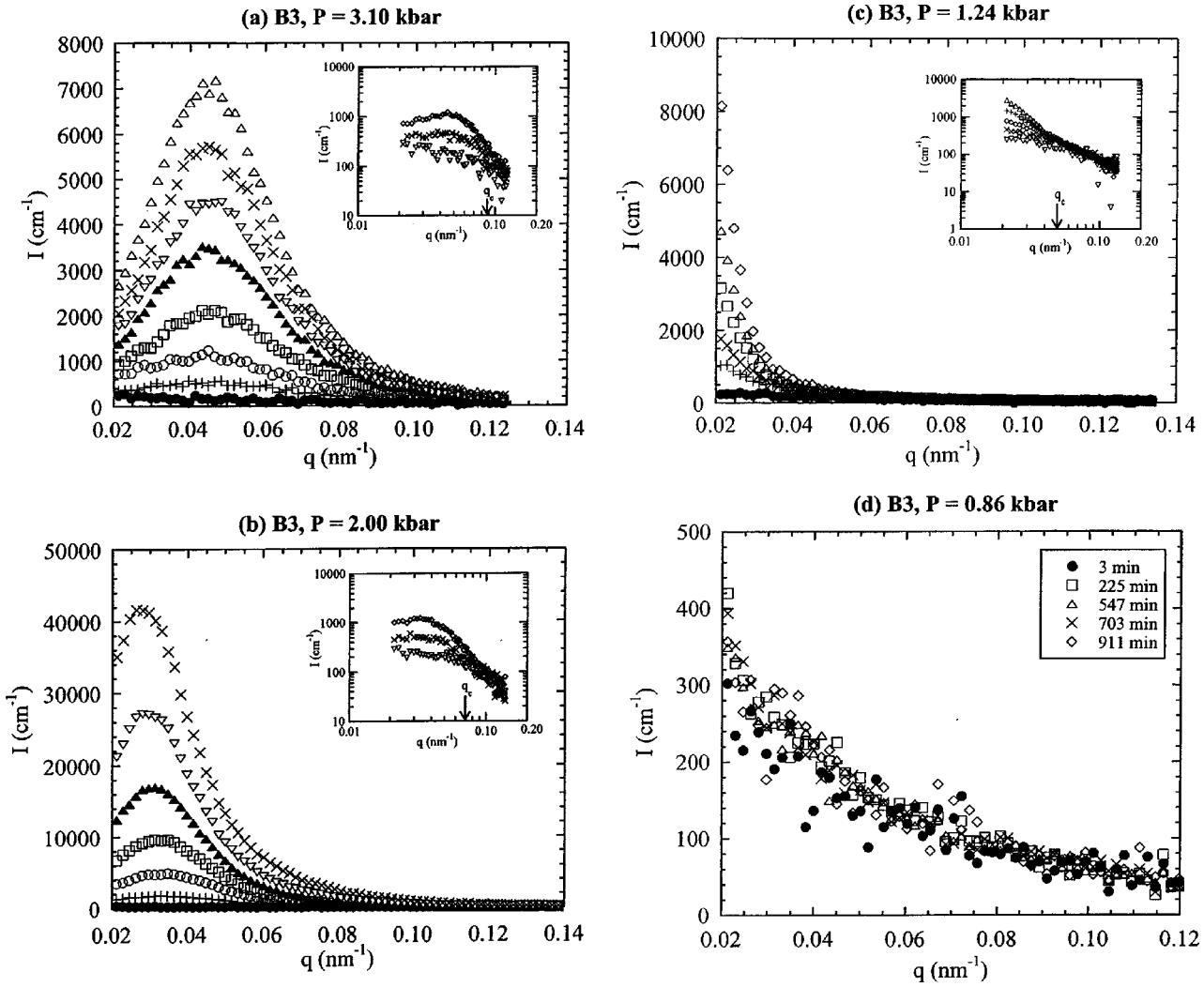

FIG. 1. The time dependence of the absolute scattering intensity, $I(q)$ vs the scattering vector, q for the B3 blend during phase separation at 58 °C and (a) 3.10 kbar, (b) 2.00 kbar, (c) 1.24 kbar, and (d) 0.86 kbar. From small to large intensity the SANS profiles are for times (a) 3 min, 77 min, 141 min, 189 min, 231 min, 252 min, 273 min, and 294 min, (b) 3 min, 153 min, 211 min, 253 min, 295 min, 337 min, and 379 min, and (c) 3 min, 475 min, 569 min, 694 min, 788 min, and 945 min. Insets: Log–log plots of $I(q)$ vs q. From small to large intensity the SANS profiles are for times (a) 5 min, 64 min, and 141 min, (b) 6 min, 58 min, and 130 min, (c) 3 min, 54 min, 412 min, 538 min, and 663 min. The arrows indicate the location of q_c, the critical scattering vector, as determined in Ref. 1.

thus obtained for the three deepest quenches is shown in Fig. 3(a).[29] At shallower quenches (2.00 kbar and 1.66 kbar) we see a clear trend toward decreasing q_p at long times. A decrease in q_p indicates coarsening of the early stage structure, or the end of the early stage where the CHC theory is expected to apply. τ_E' values for the deep quenches are thus assumed to be the time at which q_p begins to decrease with time, and are indicated by the arrows in Fig. 3(a). It is evident in Fig. 3(a) that all of the data from the deepest quench (3.10 kbar) lie within the early stage.

The dependence of q_p^2, obtained during the early stages, on quench depth is shown in Fig. 3(b). For consistency we use the largest value of q_p measured during the early stage in this plot. As in Ref. 1, we use χ/χ_s to quantify quench depth, where χ is the Flory–Huggins interaction parameter at the T and P values at which the phase separation experiments were carried out, and χ_s is the value of χ at the spinodal (throughout this paper, spinodal implies the mean-field spinodal). The

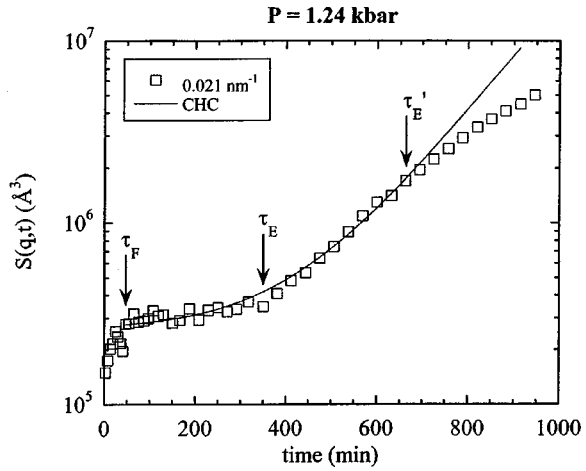

FIG. 2. The structure factor, $S(q,t)$, vs time at $q=0.021$ nm^{-1} for the 1.24 kbar quench. The solid curve is the best least-squares fit of the CHC theory [Eq. (4)] of the data for $47 \leqslant t \leqslant 664$ min. The arrows indicate τ_F, the end of the fluctuation relaxation stage, τ_E, the end of the early stage in Ref. 1, and τ_E', the end of the early stage in this work.

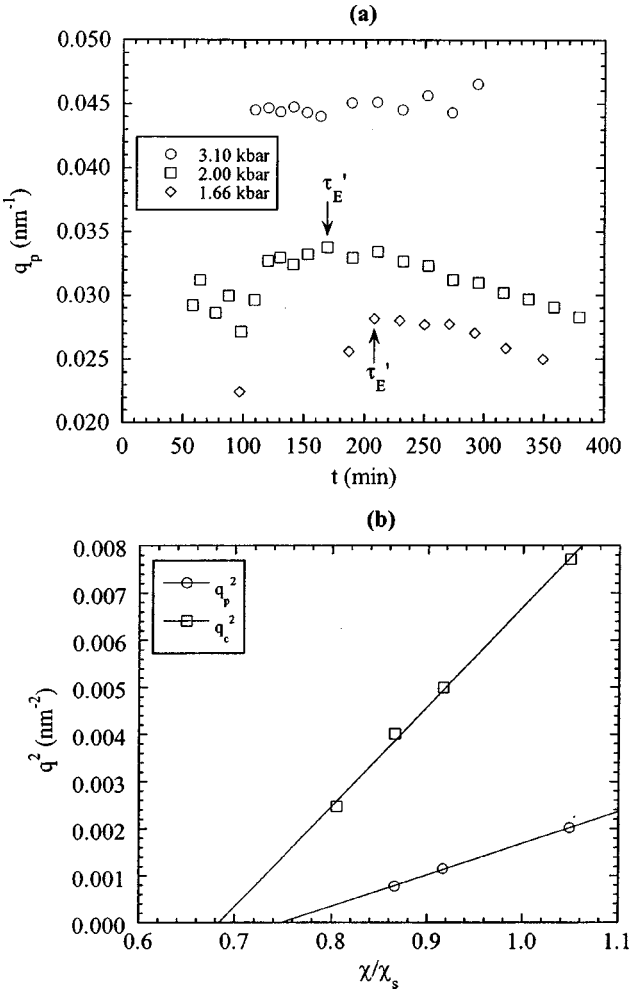

FIG. 3. (a) The q value with the largest intensity, q_p, vs time for the three deepest quenches performed on the B3 blend. The arrows indicate τ_E', the end of the early stage of phase separation for the 2.00 kbar and 1.66 kbar quenches. (b) A plot of q_p^2 and q_c^2 vs quench depth, where q_p, is the largest measured value of q_p for each quench, q_c is the critical scattering vector, χ is the Flory–Huggins interaction parameter at the quench T and P, and χ_s is the Flory–Huggins interaction parameter at the spinodal. The solid lines are the best least-squares linear fit through the data and their equations are given in the text.

relationship between the quench pressure and χ/χ_s is given in Table V of Ref. 1. Also shown in Fig. 3(b) is the dependence of q_c^2, the critical scattering vector,[1] on χ/χ_s. The dependence of both q_p^2 and q_c^2 on χ/χ_s can be approximated by straight lines: $q_p^2 = -0.00503 + 0.00673\chi/\chi_s$ and $q_c^2 = -0.0145 + 0.0212\chi/\chi_s$. Note, $q_p \to 0$ at $\chi/\chi_s = 0.75$ while $q_c \to 0$ at $\chi/\chi_s = 0.68$. It is clear that scattering peaks in $S(q,t)$ are observed well outside the spinodal ($\chi/\chi_s < 1$). In the range $0.68 < \chi/\chi_s < 0.75$ we expect scattering curves without peaks but with a critical scattering vector. The ratio q_c/q_p is about 2, regardless of quench depth.

We now analyze the full q-dependence of the measured time-dependent structure factor.

A. Shallow quench depth (1.24 kbar)

The data obtained from this quench fall into two clearly different regimes: the fluctuation relaxation stage ($0 < t < \tau_F$) and the early stage of phase separation ($\tau_F < t < \tau_E'$). The CHC theory has been used successfully to describe the decay in the concentration fluctuations when a sample is quenched from one stable homogeneous state to another.[15,16] Since the fluctuation relaxation stage is a similar response, except for the fact that the system is quenched to a metastable state, it appears reasonable to apply Eq. (4) to the fluctuation relaxation stage. In Fig. 4, we show the time dependence of $S(q,t)$ at selected q for the 1.24 kbar quench on B3 for $t \leqslant 119$ min. The solid curves through the data are the least-squares fits of the CHC equation [Eq. (4)] with $R(q)$, $S_0(q)$, and $S_t(q)$ as adjustable parameters. We chose 119 min as the upper time limit because the scattering profiles obtained between 47 min (τ_F) and 119 min were not significantly different. Also choosing a smaller upper limit (e.g., 80 min) does not have a significant effect on the results. These fits enable the determination of $R(q)$, $S_0(q)$, and $S_t(q)$. Our results are limited to $q < 0.031\ \text{nm}^{-1}$, due to the lack of change of $S(q,t)$ in the $q > 0.031\ \text{nm}^{-1}$ window. $R(q)$ obtained from the CHC analysis is shown in Fig. 5(a). As expected, $R(q)$ is negative over the entire q window. In Fig. 5(b) we show the q dependence of S_0 by filled symbols. The open symbols in Fig. 5(b) represent the first measured structure factor [$S(q, t = 3\ \text{min})$]. It is evident that $S_0(q)$ is in good agreement with the measured $S(q,t)$ at early times. Also shown in Fig. 5(b) is $S_{\text{RPA}}(q)$ at 58 °C and 0.03 kbar (solid curve), the state of the sample just prior to the quench. The agreement between $S_{\text{RPA}}(q)$ and $S_0(q)$ is significant because there are thus no adjustable parameters. In Fig. 5(c), we plot $S_t(q)$ obtained from the CHC fits, $S(q, t = 119\ \text{min})$, the structure factor at the last time used in the fits, and $S_{\text{RPA}}(q)$ at 58 °C and 1.24 kbar (solid curve). Evidently the terminal structure factor is larger in magnitude than $S_{\text{RPA}}(q)$. This indicates that the metastable ''plateau'' reached by the system as it crosses over from the fluctuation relaxation stage to the early stage of phase separation is

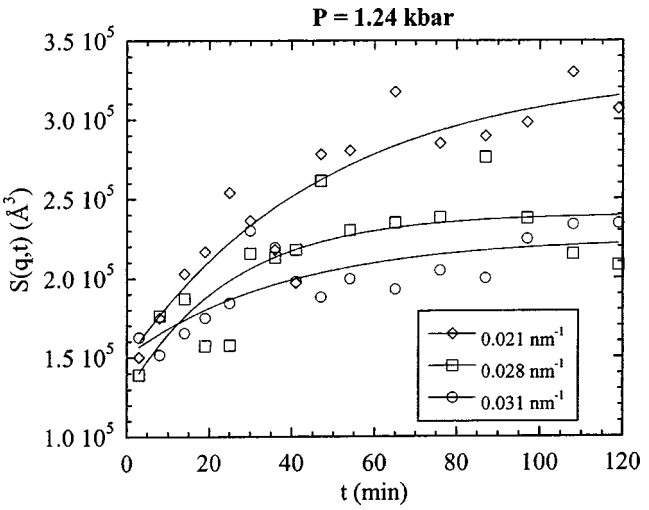

FIG. 4. The structure factor, $S(q,t)$, vs time for $t \leqslant 119$ min at selected q for the 1.24 kbar quench. The solid curves are the least-squares fits of the CHC theory [Eq. (4)] through the data. These fits enable the determination of $S_0(q)$, $S_t(q)$, and $R(q)$.

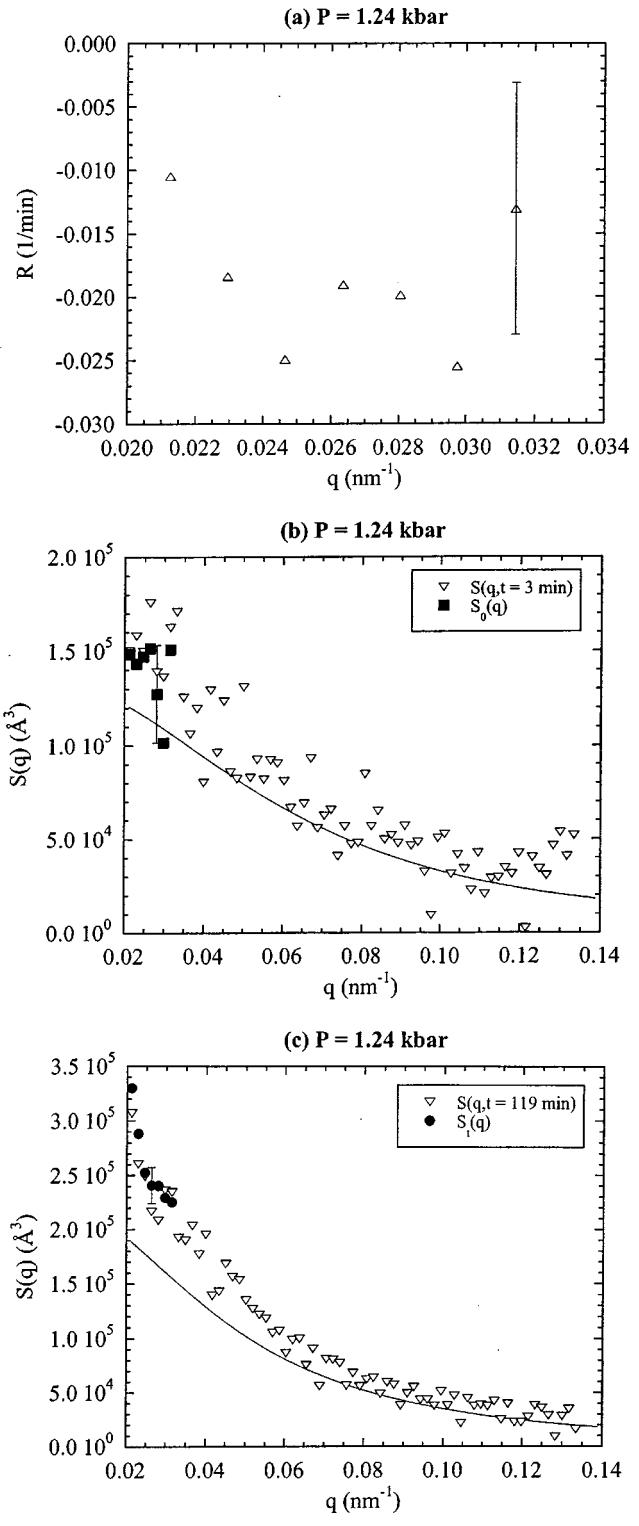

FIG. 5. The resulting fit parameters (a) $R(q)$, (b) $S_0(q)$, and (c) $S_t(q)$, vs q from the CHC fits of the data shown in Fig. 4. The solid curve in (b) and (c) is $S_{\mathrm{RPA}}(q)$ for the B3 blend at 58 °C and (b) 0.03 kbar and (c) 1.24 kbar. The error bars show the average error in the parameters.

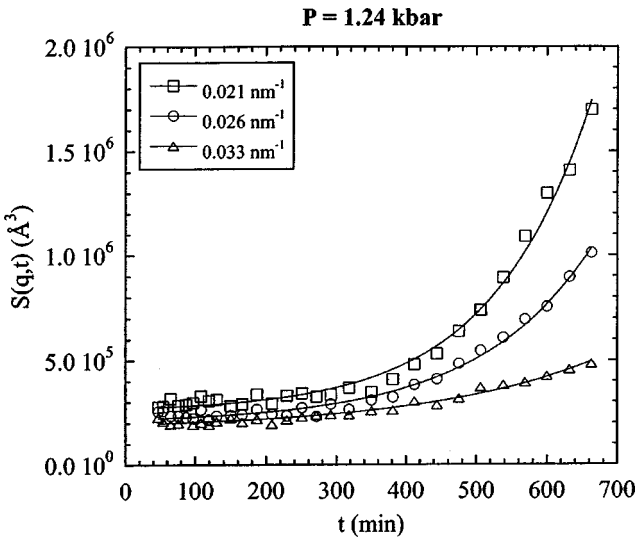

FIG. 6. The time dependence of the structure factor, $S(q,t)$, for $\tau_F \leqslant t \leqslant \tau_E'$ at selected q from the 1.24 kbar quench. The solid curves are the least-squares fit of the CHC theory [Eq. (4)] through the data. The parameters $S_0(q)$, $S_t(q)$, and $R(q)$ are determined from the fits.

characterized by larger concentration fluctuations than would be obtained if the state were stable. This increase is quantified by the difference between the data and the curve in Fig. 5(c).

In Fig. 6 we show the time dependence of $S(q,t)$ during the early stage of phase separation, $\tau_F \leqslant t \leqslant \tau_E'$ and the least-squares fits of Eq. (4) (solid curves). Of course, the CHC analysis can only be done in the regime where $S(q,t)$ increases with time and is thus limited to the $q < q_c$ range. The actual q-range over which the analysis was carried out differed slightly from q_c because the crossover from a time-dependent $S(q,t)$ to a time-independent $S(q,t)$ is not abrupt (see error bars in Fig. 9 of Ref. 1). Our analysis of the 1.24 kbar quench is thus limited to $q < 0.038\ \mathrm{nm}^{-1}$. In Fig. 7(a), we show $R(q)$ obtained from the CHC analysis.[30] Unlike the results obtained from within the fluctuation relaxation stage [Fig. 5(a)], $R(q)$ is positive and decreases continuously across the q window. The decrease in $R(q)$ with increasing q is an indication that the concentration fluctuations with smaller length scales grow more slowly. It is clear that the dynamics observed here are not consistent with a simple diffusive process, which would lead to the opposite result. Functions $S_0(q)$ and $S_t(q)$ are shown in Fig. 7(b). $S_0(q)$ and $S_t(q)$ have very similar magnitudes and decrease monotonically with increasing quench depth. In Fig. 7(c) we show $\Delta S(q) = S_0(q) - S_t(q)$. It is evident here that $\Delta S(q)$ is relatively small and appears to be independent of q in the accessible q-window.

We determined that $q_c = 0.050 \pm 0.006\ \mathrm{nm}^{-1}$ for the 1.24 kbar quench.[1] In principle, the merging of the scattering curves at q_c could be due to $\Delta S(q_c) \to 0$ and/or $R(q_c) \to 0$. Figures 7(a) and 7(c) enable resolution between these possibilities. The data in Fig. 7(a) show that $R(q)$ decreases rapidly with increasing q. A simple linear extrapolation, indicated by the line in Fig. 7(a), indicates that $R(q) \to 0$ at $q = 0.051\ \mathrm{nm}^{-1}$.[31] This is very close to the measured value of q_c. In contrast, the data in Fig. 7(c) show that $\Delta S(q)$ remains finite in our q-window. The location of q_c for the 1.24 kbar quench thus appears to be determined by $R(q)$.

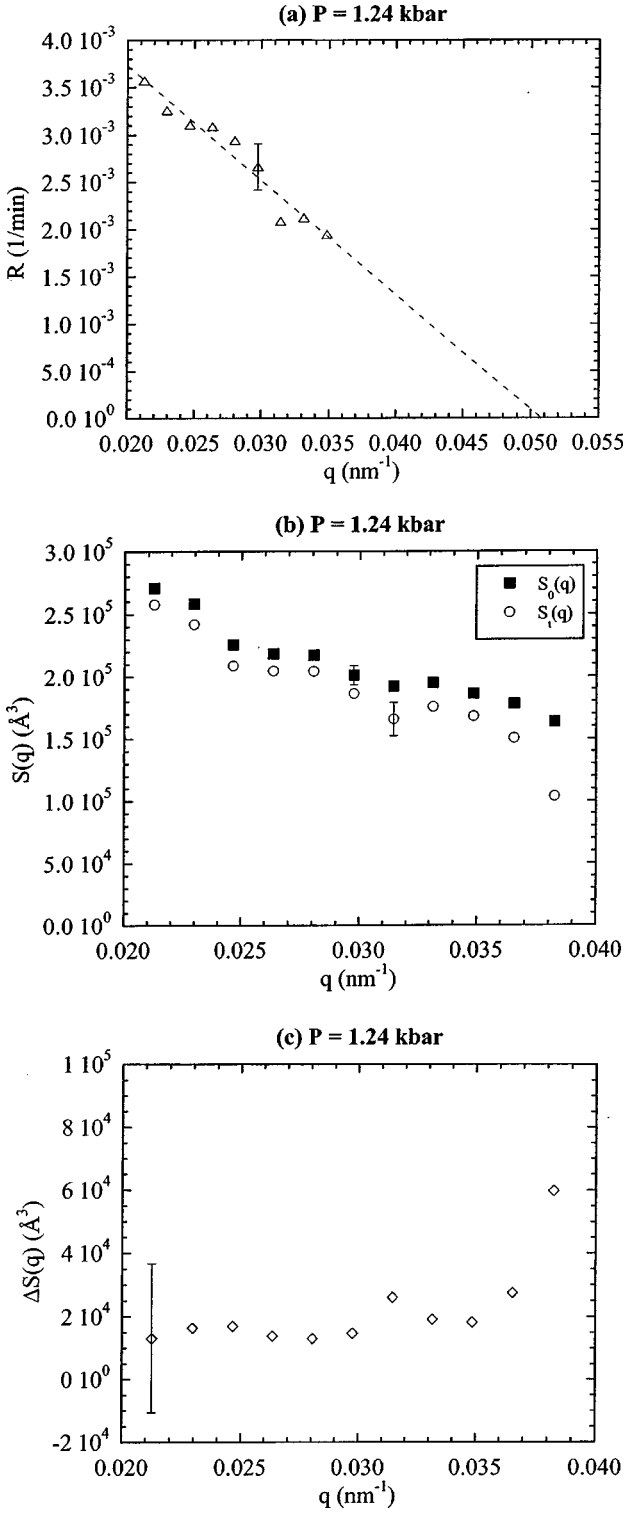

FIG. 7. The q dependence of (a) $R(q)$, (b) $S_0(q)$, and $S_t(q)$ from the fit of the CHC theory [Eq. (4)] to the 1.24 kbar quench data during the early stage (data shown in Fig. 6). The dashed line in (a) is the best least-squares linear fit of the data. (c) $\Delta S(q)$, calculated from the data in (b) vs q. The error bars show the average error in the parameters.

B. Intermediate quench depths (2.00 kbar)

The data obtained at 2.00 kbar and 1.66 kbar are similar [Figs. 1(b) and 1(c)]. For brevity, we thus discuss details of the 2.00 kbar quench only. Figure 8 shows the time dependence of $S(q,t)$ for the 2.00 kbar quench at selected q values. It is evident that the increase in $S(q,t)$ with time can be described by the CHC theory. The curves in Fig. 8 are the least-squares CHC fits through the data. The range of applicability of the CHC analysis was $q<0.085\ \mathrm{nm}^{-1}$. In Fig. 9(a) we show $R(q)$. We find that $R(q)$ increases with increasing q for $q<0.035\ \mathrm{nm}^{-1}$, and then appears to be constant at larger q. Functions $S_0(q)$, $S_t(q)$, and $S_{\mathrm{RPA}}(q)$ at 0.03 kbar and 58 °C are shown in Fig. 9(b). We find that $S_0(q)$ decreases with increasing q and is similar to $S_{\mathrm{RPA}}(q)$. It is evident, however, that $S_0(q)$ is significantly larger than $S_{\mathrm{RPA}}(q)$ over the entire q range. The reason for this difference is made clear in Fig. 9(c). The symbols in Fig. 9(c) represent typical time-dependent structure factor data and the solid curve is the least-squares CHC fit. While the CHC theory adequately describes the overall change in $S(q,t)$ with time, a systematic deviation is found at early times [$t<35$ min in Fig. 9(c)]. In this regime, indicated by the filled symbols in Fig. 9(c), the measured value of $S(q,t)$ falls below the CHC curve. It appears as though the structure factor at time zero, $S_0(q)$, is larger than the measured scattering at $t=0$. It is likely that this apparent discrepancy is due to fluctuation relaxation. It is unreasonable to expect the fluctuation relaxation stage to appear suddenly at a quench pressure of 1.24 kbar and be completely absent at higher pressures (e.g., 1.66 and 2.00 kbar). However, due to the larger quench depths at the higher pressures, we see a rapid onset of phase separation. This prevents a clear resolution of the fluctuation relaxation stage and the early stage of phase separation. We thus propose that the data obtained at very early times ($t\leqslant 34$ min) are effected by fluctuation relaxation to a metastable structure characterized by a structure factor of $S_0(q)$. As can be seen in Fig. 7(b), $S_0(q)$ is larger than that expected from a perfectly homogeneous mixture at 2.00 kbar [$S_{\mathrm{RPA}}(q)$]. In this respect, the 2.00 and 1.24 kbar quenches are similar.

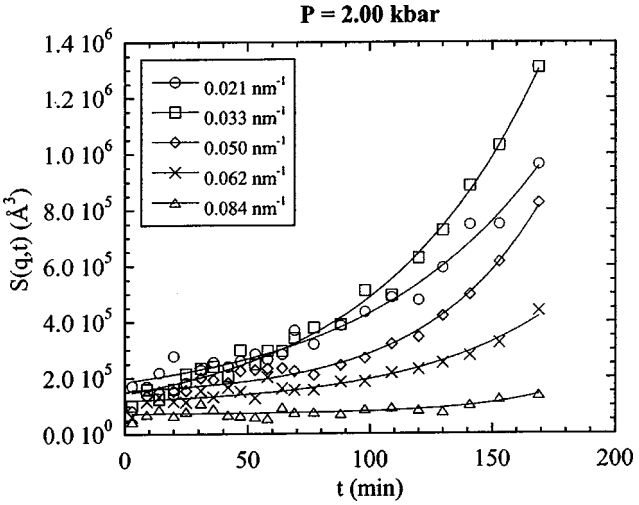

FIG. 8. The structure factor, $S(q,t)$ vs time at $t\leqslant\tau_E'$ and selected q for the 2.00 kbar quench on B3. The solid curves are the best least-squares fit of the CHC theory [Eq. (4)] through the data, enabling the determination of $S_0(q)$, $S_t(q)$, and $R(q)$.

As seen in Fig. 9(b), $S_t(q)$ at 2.00 kbar is positive over the entire q window. At $q<0.05\ \mathrm{nm}^{-1}$, $S_t(q)$ appears to be

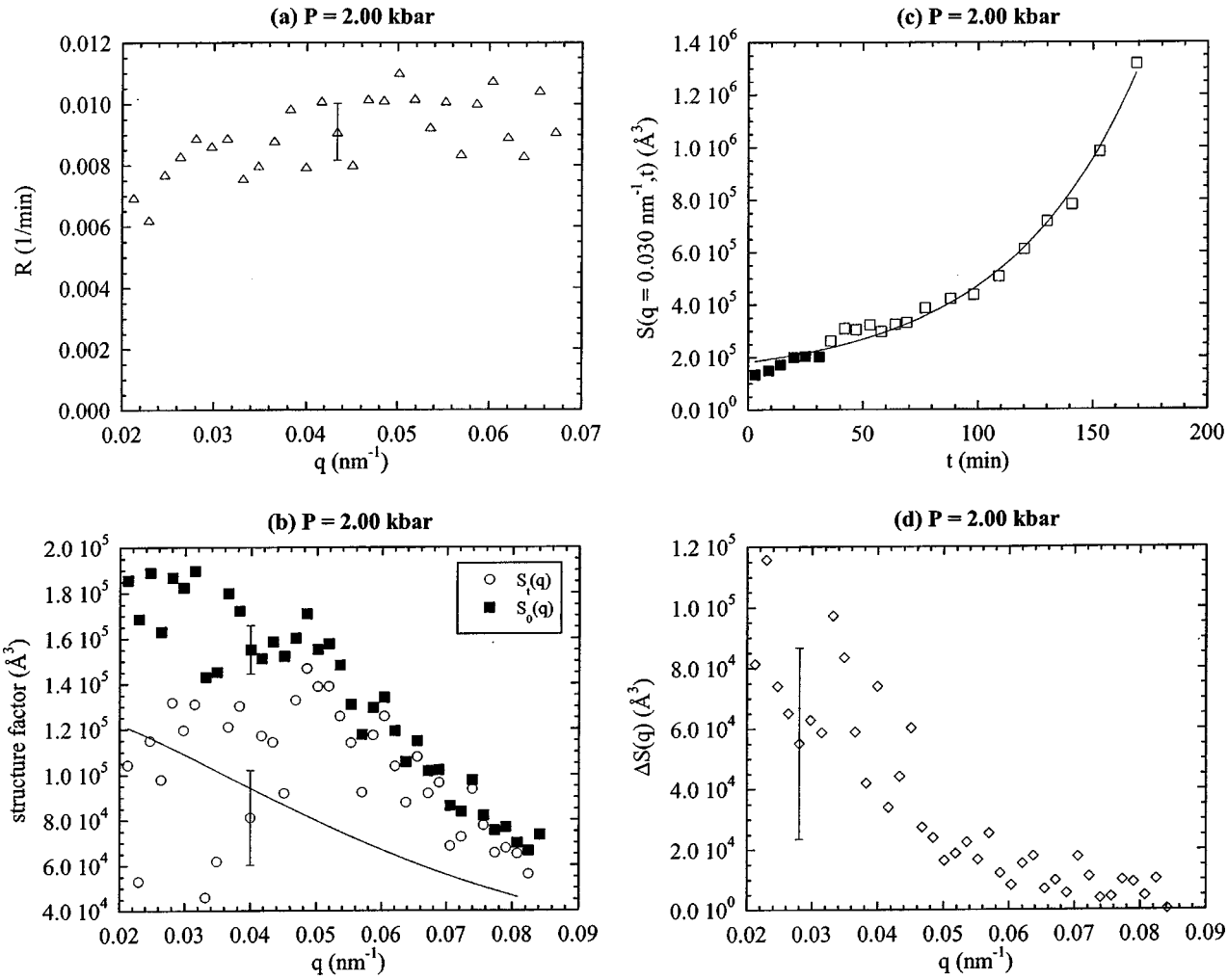

FIG. 9. The q dependence of (a) $R(q)$, and (b) $S_0(q)$, and $S_t(q)$ from the best least-squares fit of Eq. (4) to the 2.00 kbar quench data during the early stage (data shown in Fig. 8). The solid curve in (b) is $S_{\mathrm{RPA}}(q)$ at 58 °C and 0.03 kbar. (c) $S(q,t)$ vs time at $t \leqslant \tau_E'$ and $q = 0.030\ \mathrm{nm}^{-1}$ for the 2.00 kbar quench. The solid curve through the data is the least-squares fit of the CHC theory [Eq. (4)]. (d) $\Delta S(q)$, from the data shown in (b), vs q. The error bars show the average error in the parameters.

an increasing function of q (the noise in the data prevent us from being certain). At $q > 0.05\ \mathrm{nm}^{-1}$, however, $S_t(q)$ approaches $S_0(q)$ and decreases with increasing q. In Fig. 9(d), we show the q dependence of $\Delta S(q)$ for the 2.00 kbar quench. $\Delta S(q)$ is a monotonic function of q and approaches a value close to zero at $q \approx 0.07\ \mathrm{nm}^{-1}$. The value of q_c for this quench is $0.071 \pm 0.007\ \mathrm{nm}^{-1}$. The fact that $R(q)$ remains finite as $q \to q_c$ [Fig. 9(a)] indicates that the existence of a critical scattering vector at intermediate quench depths is due to the fact that $\Delta S \to 0$.

The peak in $S(q,t)$ is the most time-sensitive part of the structure factor. We thus expect $\Delta S(q)$ and/or $R(q)$ to be large in the vicinity of q_p. The simplest case would be wherein we obtain a peak in either $\Delta S(q)$ and/or $R(q)$. It is clear from Figs. 9(a) and 9(d) that this is not the case; both $\Delta S(q)$ and $R(q)$ are monotonic functions of q. However, $R(q)$ is an increasing function of q in the $q < q_p$ range [Fig. 9(a)] while $\Delta S(q)$ is a decreasing function of q in the $q > q_p$ range [Fig. 9(d)]. It is clear that the peak in $S(q,t)$ arises due to the combined effect of $R(q)$ and $\Delta S(q)$.

C. Deep quench (3.10 kbar)

The time dependence of $S(q,t)$ at selected q values during the early stage for the 3.10 kbar quench is shown in Fig. 10. The scattering intensity increases with time in a manner that is consistent with the CHC theory [Eq. (4)]. The curves in Fig. 10 are least-squares fits of Eq. (4). In Fig. 11(a), we show that $R(q)$ increases slightly from $5.5 \times 10^{-3}\ \mathrm{min}^{-1}$ to $5.8 \times 10^{-3}\ \mathrm{min}^{-1}$ with increasing $q < 0.045\ \mathrm{nm}^{-1}$ and then decreases with increasing q. In Fig. 11(b), we show that $S_0(q)$ is a positive and monotonic function of q. The curve in Fig. 11(b) is $S_{\mathrm{RPA}}(q)$ at 58 °C and 0.03 kbar (the state of the sample just prior to the quench). We find reasonable agreement between $S_0(q)$ and $S_{\mathrm{RPA}}(q)$ at this quench [similar to the agreement noted in Fig. 5(b)]. This agreement indicates the lack of importance of fluctuation relaxation in the deep quench regime. $S_t(q)$ is a nonmonotonic function of q, as seen in Fig. 11(b). It is positive at low q, and decreases with increasing q until it reaches a minimum of -5×10^{-4} Å^3 at $q \approx 0.05\ \mathrm{nm}^{-1}$, before increasing to a value close to $S_0(q)$ at

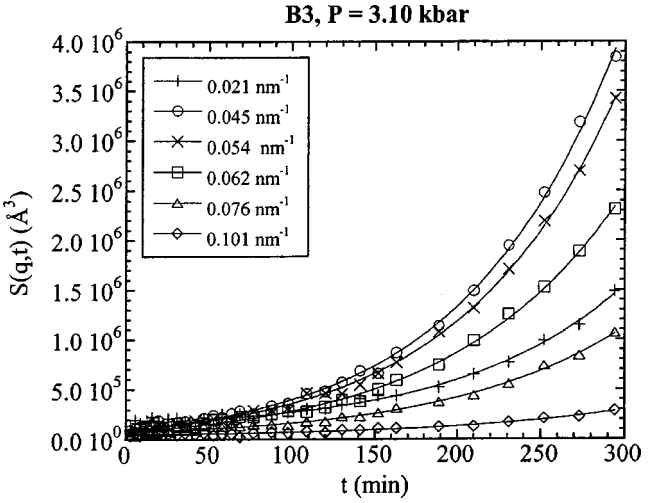

FIG. 10. The structure factor, $S(q,t)$, vs time at selected q for the 3.10 kbar quench. The solid curves are the least-squares fits of the CHC equation [Eq. (4)] through the data.

large q. $S_t(q)$ is negative over a substantial portion of our q-window, from $0.04\ \mathrm{nm}^{-1} \leqslant q \leqslant 0.07\ \mathrm{nm}^{-1}$.

The q dependence of $\Delta S(q)$ for the 3.10 kbar quench is shown in Fig. 11(c). It is evident that $\Delta S(q)$ peaks at $q \approx 0.05\ \mathrm{nm}^{-1}$. This peak is almost at the same location as the peak in $S(q,t)$; $q_p = 0.045\ \mathrm{nm}^{-1}$. It is clear that the peak in $S(q,t)$ is due mainly to the peak in $\Delta S(q)$. However, the shape and detailed location of the scattering peak is affected by the q dependence of both $\Delta S(q)$ [Fig. 11(c)] and $R(q)$ [Fig. 11(a)]. The low q side of the scattering peaks seen in the 3.10 kbar quench is mainly affected by the q dependence of $\Delta S(q)$; $R(q)$ is a weak function of q in this regime. The high q side of the scattering peaks seen in Fig. 1(a) are affected by decreases in both $\Delta S(q)$ and $R(q)$.

In Ref. 1 we determined that for the 3.10 kbar quench, $q_c = 0.088 \pm 0.006\ \mathrm{nm}^{-1}$. As is seen in Fig. 11(c), $\Delta S(q)$ decreases from its value at the peak by about two orders of magnitude as q_c is approached and at $q > q_c$ appears to approach a value close to zero. This is the same trend observed in the 2.00 kbar data [Fig. 9(d)]. In contrast $R(q)$ decreases by only about 20% between q_p and q_c. This implies that the critical scattering vector at 3.10 kbar arises due to the q dependence of ΔS and not R.

D. Applicability of Cahn analysis

We have demonstrated above that the CHC theory describes the changes in the structure factor with time during the early stages of phase separation for all of the quenches. It is expected, however, that the Cahn analysis [Eq. (6)] should be adequate at deeper quenches where $S_0(q) \gg S_t(q)$. This is demonstrated in Fig. 12, where we plot $\ln[S(q,t)]$ at $q = 0.025\ \mathrm{nm}^{-1}$ versus time for the deep quench. The line through the data represents the least-squares fit to the Cahn–Hilliard analysis [Eq. (6)]. Also shown in Fig. 12 is the time dependence of $\ln[S(q,t)]$ at $q = 0.025\ \mathrm{nm}^{-1}$ obtained at the shallow quench depth. It is clear that the Cahn analysis would fail completely in this regime. This was also true for the intermediate quench depth data. Because the CHC provides a unifying framework for analyzing all of the data and the Cahn analysis does not, we have focused on the results obtained from the CHC analysis.

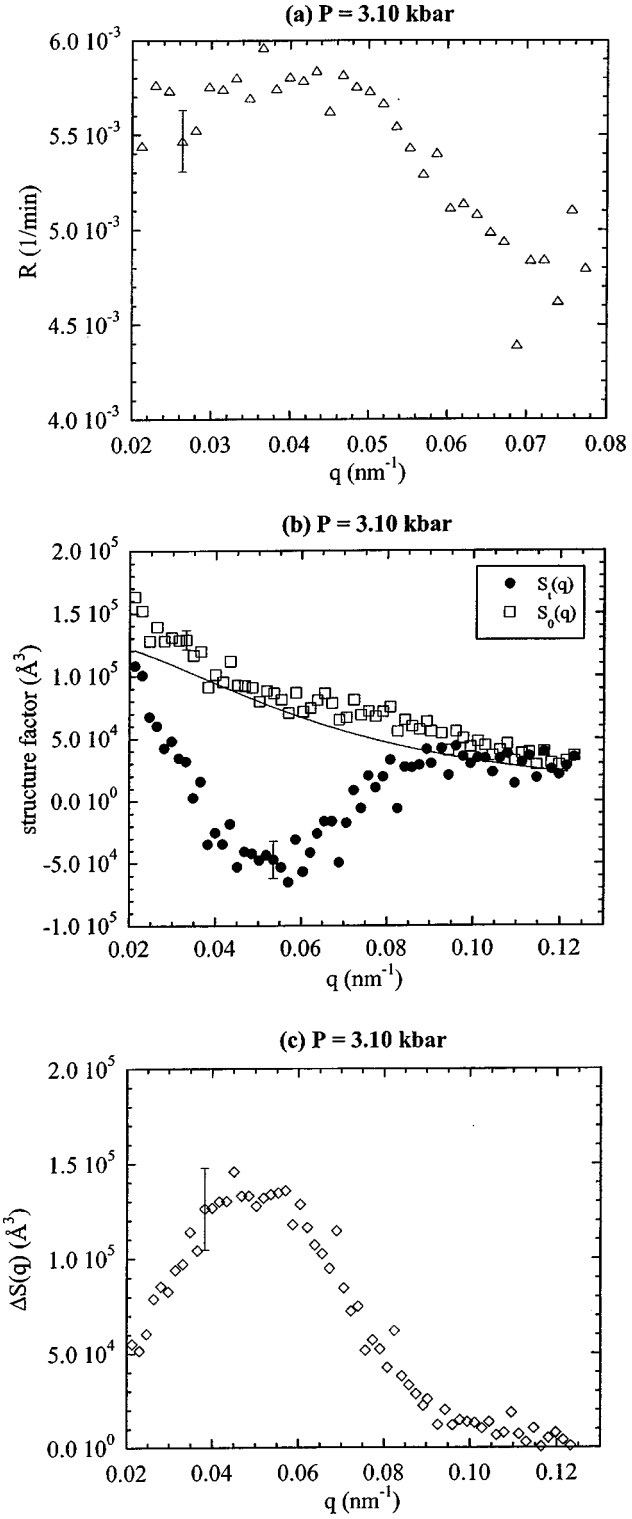

FIG. 11. The q dependence of (a) $R(q)$, and (b) $S_t(q)$, and $S_0(q)$ from the least-squares fit of the CHC theory [Eq. (4)] to the 3.10 kbar quench data (data shown in Fig. 10). (b) The solid curve is $S_{\mathrm{RPA}}(q)$ at 58 °C and 0.03 kbar. (c) $\Delta S(q)$, calculated from the data in (b), vs q. The error bars show the average error in the parameters.

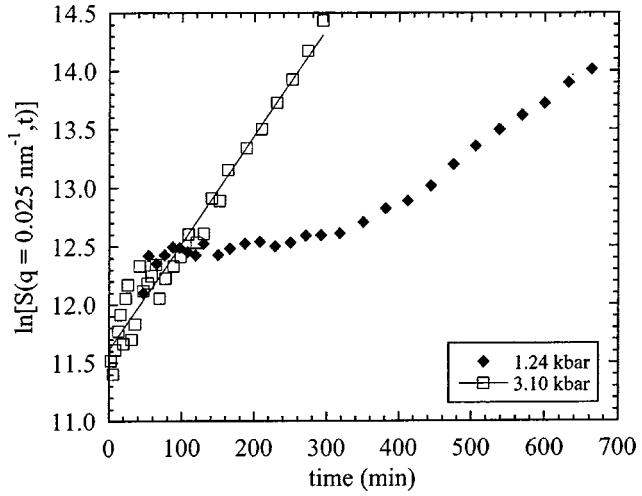

FIG. 12. The time dependence of $\ln[S(q,t)]$ at $q=0.025\ \mathrm{nm}^{-1}$ for the 1.24 kbar and 3.10 kbar quenches during the early stage. The solid line is best least-squares linear fit through the 3.10 kbar data.

V. CONCLUSION

The Cahn–Hilliard–Cook theory was used to analyze the evolution of off-critical, binary polyolefin blends quenched into the metastable region of the mean-field phase diagram. The dynamics are characterized by obtaining the time-dependent structure factor $S(q,t)$ from SANS measurements. The rich variety of time dependencies, seen in Fig. 1, are recast in terms of three q-dependent but time-independent parameters: $S_0(q)$, the initial structure factor, $S_t(q)$, the terminal structure factor, and $R(q)$, the rate of growth of the structure factor. At deep quenches, $S_0(q)$ is identical to that predicted by the RPA at the quench conditions. As quench depth decreases, we see the gradual appearance of a fluctuation relaxation stage prior to phase separation. The distinction between the fluctuation relaxation stage and the early stage of phase separation becomes clearer with decreasing quench depth. The structure factor at the end of the fluctuation relaxation stage is larger than that predicted by the RPA. Metastable states formed at shallow and intermediate quench depths thus have fluctuations that are somewhat larger in magnitude than those that would be obtained if the sample were at equilibrium. It is evident, however, that the RPA provides a reasonable starting point for the understanding of $S_0(q)$.

There are no theories that address functions $R(q)$, and $S_t(q)$. The effect of quench depth on these functions is summarized in Fig. 13. We use qR_g as the abscissa in Fig. 13 because this combination occurs naturally in many known static and dynamic structure factors. R_g, the radius of gyration of our polymers, is 16 ± 1 nm. It is well-known that phase transition kinetics are affected by both thermodynamic driving forces and kinetic factors such as the viscosity of the medium. This leads to a maximum in phase separation kinetic rates at intermediate quench depths. Evidence for such a maximum is clearly seen in Fig. 13(a). The magnitude of R, which is a measure of the rate of the phase separation, is largest at intermediate quench depth, $\chi/\chi_s=0.92$. The dependence of R on qR_g shows the following systematic trends

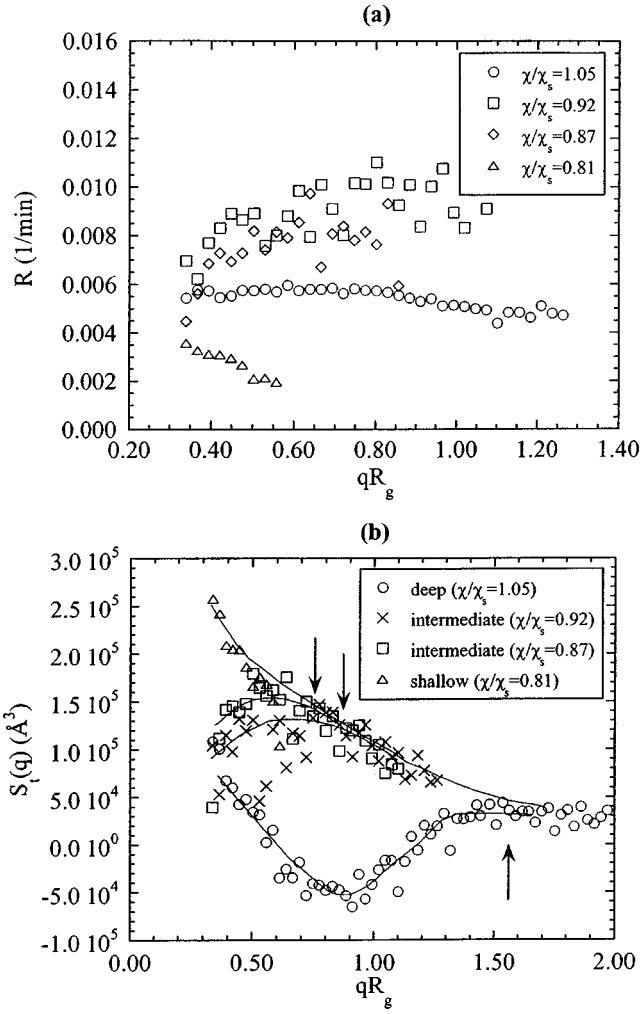

FIG. 13. The dependence (a) R and (b) S_t on qR_g for all of the quenches on the B3 blend, where R_g is the radius of gyration of the polymers. The legend gives the value of χ/χ_s for each quench. The correspondence between the quench T and P and χ/χ_s is given in Table V in Ref. 1. (b) The arrows indicate where the intermediate and deep quenches deviate from the universal curve.

with quench depth: R is independent of qR_g during deep quenches, increases with qR_g at intermediate quench depths and, decreases with qR_g at shallow quench depths. Of particular interest is the fact that $R\rightarrow0$ as $q\rightarrow q_c$ at shallow quench depths. In contrast, S_t shows unremarkable, monotonic behavior at shallow quench depths and more interesting behavior at deep quench depths. This is shown in Fig. 13(b). At large qR_g, S_t approaches a universal curve that is qualitatively similar to that predicted by the RPA structure factor. The S_t curves deviate from this universal curve at qR_g values that increase with increasing quench depth. The arrows in Fig. 13(b) indicate the qR_g values where these deviations become evident. For deep and intermediate quenches these deviations are evident in the vicinity of $q\approx q_c$. The magnitude of the deviations increases with increasing quench depth leading to a minimum at the deepest quench depth in the vicinity of $qR_g=1$ and negative terminal structure factors over a substantial portion of our qR_g-window.

We hope that our observation of trends in $R(qR_g)$,

$S_0(qR_g)$, and $S_t(qR_g)$ will guide the development of theories that address the thermodynamics and kinetics of phase separation of blends near the metastability limit.

While some aspects of the data presented here and the preceding paper[1] are explained by the Wang–Wood theory,[3,4] many fundamental questions regarding phase separation kinetics in polymer blends remain unanswered. For example, it is not clear if we should consider our quenched blends as metastable or unstable. In the Wang–Wood theory, the spinodal is suppressed to 0 K. This conclusion, is however, clouded by the fact that the Wang–Wood theory breaks down well above the spinodal temperature at the metastability limit. If the Wang–Wood conclusion regarding the spinodal is correct then it indicates that our experiments pertain to the evolution of structure in metastable blends. The applicability of the CHC analysis leaves little doubt that concentration fluctuations play an important role in the systems that we have studied. Our observations of a time independent scattering peak, a negative terminal structure factor, and the applicability of the Cahn analysis in the deep quench regime, suggest that we might have crossed the stability limit. Thus the very existence of a stability limit in off-critical polymer blends remains unresolved.

The Wang–Wood theory does provide valuable guidance for constructing systems for studying the initial stages of nucleation above the metastability limit and outside the Ginzburg regime. Such a system would enable a rigorous test of classical nucleation concepts such as divergence of R_c as the spinodal is approached. We have been unable to observe any signs of nucleation in any of the experiments that we have conducted above the metastability limit and outside the Ginzburg regime [e.g., 0.86 kbar quench in Fig. 1(d)]. This indicates that the nucleation barriers cannot be overcome in a reasonable amount of time in high molecular weight polymer blends in this regime. In the future we plan to use the Wang–Wood theory to design systems with lower nucleation barriers and thereby study the formation of critical nuclei in metastable blends where fluctuations are unimportant.

ACKNOWLEDGMENTS

We thank the National Science Foundation (Grant No. CTS-0196066) for financial support. We acknowledge the support of the National Institute of Standards and Technology, U.S. Department of Commerce, in providing facilities used in this work. The SANS instrument is supported by Grant No. DMR-9986442 from the National Science Foundation to NIST (Ref. 32).

[1] A. A. Lefebvre, J. H. Lee, N. P. Balsara, and C. Vaidyanathan, J. Chem. Phys. **117**, 9063 (2002).
[2] J. W. Cahn and J. E. Hilliard, J. Chem. Phys. **31**, 688 (1959).
[3] Z. G. Wang, J. Chem. Phys. **117** 481 (2002).
[4] S. M. Wood and Z. G. Wang, J. Chem. Phys. **116**, 2289 (2002).
[5] J. W. Cahn, J. Chem. Phys. **42**, 93 (1965).
[6] H. E. Cook, Acta Metall. **18**, 297 (1970).
[7] K. Binder, J. Chem. Phys. **79**, 6387 (1983).
[8] A. A. Lefebvre, J. H. Lee, N. P. Balsara, and B. Hammouda, J. Chem. Phys. **116**, 4777 (2002).
[9] A. A. Lefebvre, J. H. Lee, H. S. Jeon, N. P. Balsara, and B. Hammouda, J. Chem. Phys. **111**, 6082 (1999).
[10] N. P. Balsara, C. C. Lin, and B. Hammouda, Phys. Rev. Lett. **77**, 3847 (1996).
[11] J. S. Higgins and H. C. Benoît, *Polymers and Neutron Scattering* (Oxford University Press, Oxford, 1994).
[12] P. G. de Gennes, *Scaling Concepts in Polymer Physics* (Cornell University Press, Ithaca, 1979).
[13] A. A. Lefebvre, J. H. Lee, N. P. Balsara, and C. Vaidyanathan, Macromolecules **35**, 7758 (2002).
[14] A. A. Lefebvre, J. H. Lee, N. P. Balsara, and B. Hammouda, Macromolecules **33**, 7977 (2000).
[15] Y. Feng, C. C. Han, M. Takenaka, and T. Hashimoto, Polymer **33**, 2729 (1992).
[16] G. Merkle, B. J. Bauer, and C. C. Han, J. Chem. Phys. **104**, 9647 (1996).
[17] M. Okada and C. C. Han, J. Chem. Phys. **85**, 5317 (1986).
[18] D. Schwahn, K. Hahh, J. Streib, and T. Springer, J. Chem. Phys. **93**, 8383 (1990).
[19] M. He, Y. Liu, Y. Feng, M. Jiang, and C. C. Han, Macromolecules **24**, 464 (1991).
[20] T. Hashimoto, M. Takenaka, and T. Izumitani, J. Chem. Phys. **97**, 679 (1992).
[21] D. Schwahn, S. Janssen, and T. Springer, J. Chem. Phys. **97**, 8775 (1992).
[22] H. Jinnai, H. Hasegawa, T. Hashimoto, and C. C. Han, J. Chem. Phys. **99**, 4845 (1993).
[23] H. Jinnai, H. Hasegawa, T. Hashimoto, and C. C. Han, J. Chem. Phys. **99**, 8154 (1993).
[24] G. Müller, D. Schwahn, H. Eckerlebe, J. Rieger, and T. Springer, J. Chem. Phys. **104**, 5326 (1996).
[25] J. W. Cahn and J. E. Hilliard, J. Chem. Phys. **28**, 258 (1958).
[26] K. B. Rundman and J. E. Hilliard, Acta Metall. **15**, 1025 (1967).
[27] T. Nishi, T. T. Wang, and T. K. Kwei, Macromolecules **8**, 227 (1975).
[28] F. S. Bates and P. Wilzius, J. Chem. Phys. **91**, 3258 (1989).
[29] It is sometimes difficult to identify peaks in the presence of finite signal to noise ratio. The missing data in Fig. 3(a) imply that a scattering peak was not identifiable (especially at early times), or Eq. (7) led to q_p being located at $q<0.021\ \mathrm{nm}^{-1}$, the lower limit of our q window.
[30] The error bars indicate the average error in $R(q)$ for the data shown. We omit the data at higher q because the error in R was at least 1.5 times greater than the error bar shown. It was also difficult to discern trends in the data in this higher q window due to the large amount of noise.
[31] In reality, R should be a function of q^2. However within the precision of our measurements, the least-squares line shown is an accurate description of the data.
[32] Identification of equipment and materials does not imply recommendation by the National Institute of Standards and Technology.